Environmental Science & Technology

pubs.acs.org/est

Article

Size and Structure-Dependent Molecular Fingerprint Transformation of Microplastic-Derived Dissolved Organic Matter in Sunlit Seawater: Implication for Marine Carbon Cycles

Yan-Jun Liu, Zhao Liang Chen,* Zekun Zhang, Yuanbi Yi, Ruanhong Cai, Ming Ye, Mengyang Liu, Meng Yan, Kenneth Mei Yee Leung, Tanveer M. Adyel, and Ding He*

Cite This: *Environ. Sci. Technol.* 2025, 59, 18846−18856

Read Online

ACCESS | Metrics & More | Article Recommendations | Supporting Information

ABSTRACT: Microplastics (MPs) widely pollute marine environments, where the release of MPs-derived dissolved organic matter (MPs-DOM) induced by UV irradiation has been widely documented. However, the effect of MPs' inherent properties on photochemical transformation of MPs-DOM and its implication for oceanic carbon cycles remain poorly understood. Herein, we conducted 180 day artificial weathering experiments under sunlit seawater using polyethylene (PE) and polypropylene (PP) with different sizes as models, investigating the temporally dynamic features of MPs-DOM. Results showed that PP can release more MPs-DOM than PE, and concentrations of MPs-DOM derived from small-sized MPs (~250 μm) were 2−6 times higher than those of large-sized MPs (~5 mm). Spectroscopy and ultrahigh-resolution mass spectrum further revealed that protein-like substances can be persistently produced from MPs with lower photochemical activity (i.e., PE and large-size PP), while DOM derived from MPs with higher photochemical activity (i.e., small-size PP) could be gradually transformed from biolabile components to biorecalcitrant molecules. Furthermore, the persistently accumulated molecules were matched and projected onto an aquatic DOM database, and their relative intensity exhibited a gradually increasing trend across the river-to-ocean continuum at the molecular level. This work reveals the structure−reactivity relationships for MPs-DOM transformation and highlights MPs' potential impact in marine organic carbon cycles.

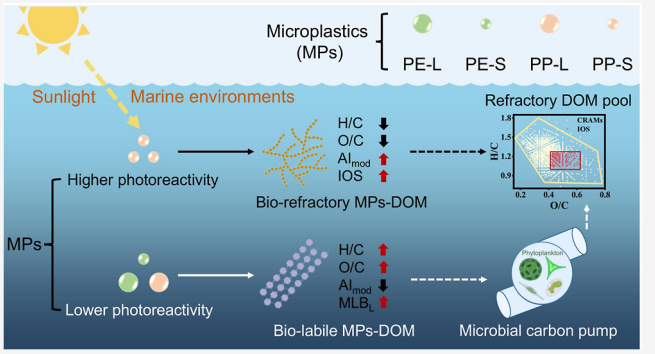

KEYWORDS: *microplastics, dissolved organic matter, UV-irradiation, FT-ICR MS, dynamic molecular transformation, marine environments*

INTRODUCTION

Plastics widely used in all aspects of daily life are typical indicators of the Anthropocene.[1] The global plastic production increased from 62 million tons in 1979 to 414 million tons in 2023.[2] The tremendous use of plastic products and improper management regulations caused massive accumulation of plastic waste in natural environments.[3] Notably, a large fraction of plastic debris inevitably enters rivers along with rainfall and surface runoff and finally reaches and persists in marine ecosystems.[4] It is estimated that 1.15−2.41 million tons of plastic waste is transported into the oceans per year.[5] Plastics in marine ecosystems undergo various natural processes and break down into particles of smaller sizes, such as microplastics (MPs, <5 mm).[6] The widely distributed MPs are considered as emerging contaminants due to their potential risks to marine biota and public health.[7] For instance, MPs could be mistakenly ingested by aquatic organisms and even enter the human body via the food chain, leading to adverse effects including mechanical injury, inflammatory response, and metabolic disturbance.[8−10] Further, MPs can also affect the fate and transport of antibiotic resistance genes, opportunistic pathogens, and chemical pollutants (e.g., organic contaminants and heavy metals) in seawater due to their huge specific surface area and stronger hydrophobicity.[11−13] Although these works suggest that MPs are indeed capable of inducing a negative impact at the ecosystem level, the crucial role of MPs in biogeochemical cycling (e.g., organic carbon turnover) in marine environments still remains unclear.

Ocean dissolved organic matter (DOM) is one of the largest active carbon pools on the earth (662 Pg C), and it is similar in quantity to the atmospheric CO_2 (828 Pg C).[14] Ocean DOM

Received: March 27, 2025
Revised: July 31, 2025
Accepted: August 1, 2025
Published: August 9, 2025

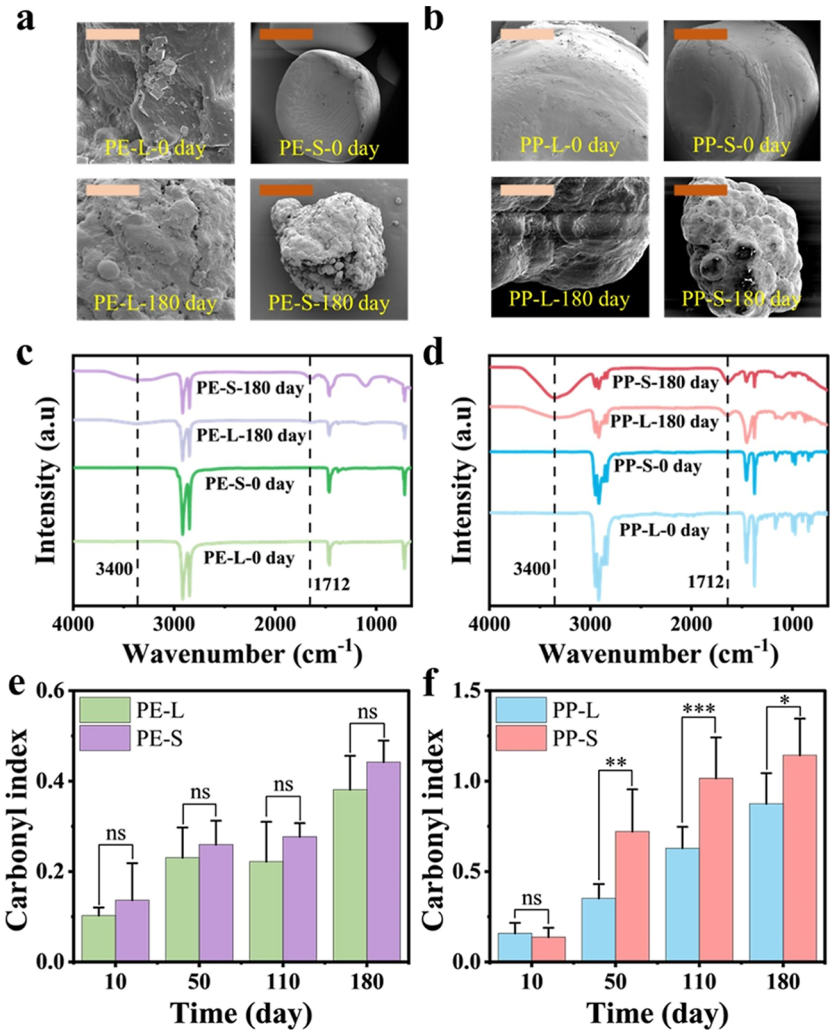

Figure 1. Physicochemical properties of MPs before and after aging. Representative SEM images of (a) PE and (b) PP before and after 180 day aging. Scale bars in SEM images of large (i.e., PE-L and PP-L) and small (i.e., PE-S and PP-S) MPs are 1 mm and 100 μm, respectively. FTIR spectra of (c) PE and (d) PP before and after 180 day aging. Variation of the carbonyl index of (e) PE and (f) PP under 10, 50, 110, and 180 day aging. Data were expressed as mean ± standard deviation (n = 5). A significant difference is indicated at the *P < 0.05, **P < 0.01, or ***P < 0.001 level ("ns" represents not significant).

is mainly derived from two sources: autochthonous (e.g., algal and microbial metabolites) and allochthonous (e.g., terrestrial input and anthropogenic activities).[15] A previous study reported that approximately 5.25 trillion MPs derived from anthropogenic activities are floating at the sea surface, contributing to 260−23,600 tons of dissolved organic carbon (DOC) annually.[16] Notably, the release of MPs-derived DOM (MPs-DOM) is closely linked with various degradation processes, such as mechanical abrasion, photo/thermal-oxidation, and microbial degradation. Bio- and thermo-degradations are slow compared to sunlight-driven photo-degradation under ocean conditions, making sunlight exposure the dominant pathway responsible for MP degradation and MPs-DOM release in surface seawaters.[17,18] Although the photodegradation of plastics into DOM is widely recognized, some limitations regarding the dynamic turnover of MPs-DOM still exist. For instance, the exposure time of MP photodissolving into MPs-DOM was largely confined to 60 days in documented experimental studies, while MPs in natural marine environments can persist for much longer.[19−21] As a result, the dynamic molecular characteristics of MPs-DOM during long-term plastic photodegradation are largely unknown. In addition, prior studies mainly focused on the effects of plastic types on MPs-DOM leaching, and the particle size of MPs was barely considered. It is well-known that the surface-to-volume ratio of the particle increases with decreasing particle size, which might increase the contact interface between MPs and light and consequently accelerate MP photodegradation and MPs-DOM release.[16] However, the effect of MPs size on MPs-DOM leaching has not been well characterized. Therefore, this study was designed to investigate the influence of chemical structure and size of MPs on the molecular fingerprint transformation of MPs-DOM under long-term UV irradiation and elucidate the role of MPs-DOM in global marine carbon cycles.

Specifically, we conducted 180 days of artificial weathering experiments under sunlit seawater to study the dynamic molecular characteristics of MPs-DOM using polyethylene (PE) and polypropylene (PP) with different sizes. These two types of MPs were selected since they are dominated buoyant MPs (densities lower than seawater) and consequently more prone to sunlight exposure.[22,23] The surface morphology and

https://doi.org/10.1021/acs.est.5c04083
Environ. Sci. Technol. 2025, 59, 18846−18856

chemical functional groups of virgin and weathered MPs were characterized by scanning electron microscopy (SEM) and Fourier transform infrared spectroscopy (FTIR). Subsequently, the molecular compositions of MPs-DOM under long-term MP photodegradation were further determined with three-dimensional excitation−emission matrix fluorescence analysis (3D-EEM) and Fourier transform-ion cyclotron resonance mass spectrometry (FT-ICR MS). Lastly, characteristic components of MPs-DOM with a significantly upward trend (relative intensity-increased molecules along with aging period) were selected to match our established DOM molecular fingerprint database and projected into global typical water environments.[24] Based on the above characterizations and analyses, we aimed to (i) reveal the effects of chemical structure and size on the photoaging of MPs and photochemical transformation of MPs-DOM; (ii) track temporally dynamic features of MPs-DOM during persistent weathering periods in sunlit seawater; and (iii) illuminate the potential implication of MPs-DOM for marine carbon cycles. Overall, this study deepens our understanding of MPs-DOM molecular fingerprints under long-term sunlight, providing valuable insights for marine organic carbon cycles.

MATERIALS AND METHODS

Chemicals. Two types of MPs (i.e., PE and PP) with diameters of ∼5 mm and ∼250 μm, namely, PE large (PE-L), PE small (PE-S), PP large (PP-L), and PP small (PP-S), were purchased from Yangli Electromechanical Technology Co. Ltd. (Shanghai, China). Infrared spectroscopy and scanning electron microscopy of these MPs were conducted to confirm the polymer types and surface morphology (Figure 1). All MPs were thoroughly washed with alcohol and deionized water three times to remove residual organic substances before use. These MPs were chosen based on their prevalence in the global plastic market, with PE and PP accounting for 26.3% and 18.9% of total plastic demand, respectively, ranking them first and second.[2] In addition, these two types of MPs were widely detected in global surface seawater owing to their lower densities (∼0.9 g/cm^3), making them more prone to sunlight irradiation.[23] Other analytical grade chemicals purchased from Sinopharm Chemical Reagent Co., Ltd. (Shanghai, China) were used without further purification. To prepare the artificial seawater (see detailed chemical composition in Table S1), electrolytes were weighted and dissolved in ultrapure water (resistivity >18.2 MΩ·cm) and filtered through a 0.22 μm filter membrane.

Aging Experiment. The aging experiments were conducted according to our previous study.[25] Briefly, pristine MPs were exposed to continuous UVA irradiation (0.3 mW/cm^2, 365 nm) for 180 days under artificial seawater to simulate long-term coastal photoaging. Such UVA intensity was comparable to the radiation intensity in the Hong Kong coastal surface seawater at 1 m depth.[25] Suspension withdrawn on days 7, 14, 21, 28, 35, 50, 90, 110, 130, 150, and 180 were filtered and stored in the dark at 4 °C before analysis. The detailed experimental workflow, including the artificial weathering process and subsequent characterization measurements, is illustrated in Texts S1 and S2, Figure S1.

DOC and Spectrometry Analyses. The DOC concentration of each sample was measured by a total organic carbon analyzer (TOC-L, Shimadzu, Japan) after being filtered through a 0.22 μm filter and acidification to pH 2. In addition, leachates collected during the aging period were subjected to 3D-EEM using a fluorescence spectrometer (Duetta, Horiba, Japan). A series of emission spectra from 255 to 500 nm with 0.5 nm intervals were collected over excitation wavelengths ranging from 250 to 500 nm by 5 nm increment. Three fluorescent indices, including the fluorescent index (FI), biological index (BIX), and humic index (HI), were calculated based on the EEM spectra.[26,27] Furthermore, the parallel factor analysis (PARAFAC) was performed using R package staRdom to determine the variation of fluorescent components among samples.[28] The detailed procedures are described in Text S3.

FT-ICR MS Analysis. The filtered samples were concentrated by solid phase extraction (SPE) with Agilent Bond Elute PPL cartridge (200 mg, 3 mL), while the blank was prepared with artificial seawater following the same procedures.[29] Detailed sample preparations are provided in Text S4. The obtained SPE-DOM samples were measured using FT-ICR MS (Solarix, Bruker Daltonik GmbH, Bremen, Germany) equipped with a 15 T superconducting magnet, which was operated with an electrospray ionization (ESI) source in negative mode. The acquired ultrahigh-resolution mass spectra with the range of 150−1000 m/z were subjected to internal calibration, peak alignment, and formula assignment using our in-house code.[30] Herein, the potential formulas were composed of $^{12}C_{1-100}{}^{1}H_{1-200}{}^{16}O_{1-40}{}^{14}N_{0-3}{}^{32}S_{0-2}{}^{31}P_{0-1}$ with a signal-to-noise ratio >6 and absolute mass detection errors of <1 ppm. To confirm the MPs-DOM specificity, the molecules detected in artificial seawater were removed from UV-exposure MP samples. Based on the identified formulas, the key parameters for data analysis were determined according to prior literature: H/C ratio, O/C ratio, double bond equivalence (DBE), modified aromaticity index (AI_{mod}), and nominal oxidation state of carbon (NOSC).[31−33] All of the indexes in this study were intensity-weighted values. Furthermore, the calculated H/C ratio and O/C ratio were applied to divide compounds into seven molecular groups.[34] The detailed calculation processes and component classification are described in Text S5.

To further understand the change of DOM molecular characteristics during aging periods, we introduced a series of indicators, including carboxyl-rich alicyclic molecules (CRAMs) (higher values represent greater DOM stability), a molecular stability boundary labile (MLB_L) (higher values indicate greater biodegradability), and island of stability (IOS) (higher values indicate greater DOM recalcitrancy).[35−37] In addition, the ultrahigh mass resolution of FT-ICR MS data makes it feasible to infer biochemical transformations of molecules.[38] Hence, we calculated mass differences between FT-ICR MS peaks to further evaluate the biochemical transformation potential for each molecule.[39] All possible pairwise mass differences were compared with a transformation database and then counted for each molecule to classify the molecular activity. The open algorithm and database for calculating biochemical transformations can be found at https://github.com/danczakre/Meta-Metabolome_Ecology. Subsequently, the DOM assemblages were divided into four contrasting partitions by considering reactivity and activity.[40] It should be noted that only the relative intensity-increased MPs-DOM molecules during the aging period were subjected to biochemical transformation potential analysis. The detailed definition and classification of each fraction are presented in Text S6.

Molecular Database. The synthesized molecular fingerprint database comprises 2853 water samples from previous

https://doi.org/10.1021/acs.est.5c04083
Environ. Sci. Technol. 2025, 59, 18846−18856

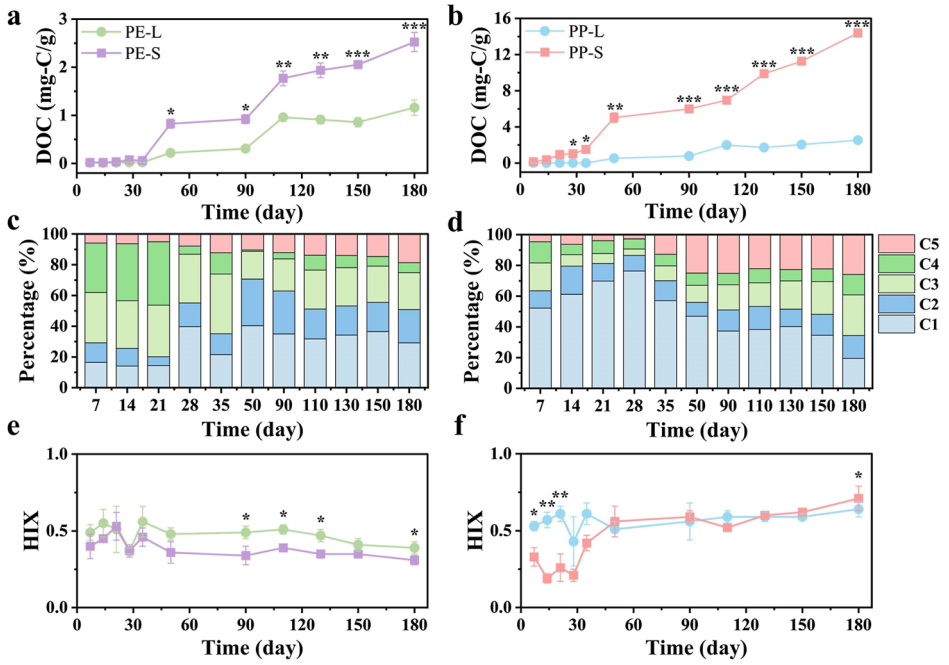

Figure 2. Changes of DOC contents and fluorescent components. Variation of weight-normalized DOC concentrations of (a) PE and (b) PP MPs-DOM under 180 day artificial weathering. Relative abundance of fluorescent components (C1−C5) calculated by the PARAFAC modeling for (c) PP-L and (d) PP-S MPs-DOM under 180 day artificial weathering. Variation of HIX of (e) PE and (f) PP MPs-DOM under 180 day artificial weathering. Data were expressed as mean ± standard deviation (n = 3). Significance analysis is conducted between large (PE-L/PP-L) and small (PE-S/PP-S) MPs at the same time point. A significant difference is indicated at the *P < 0.05, **P < 0.01, or ***P < 0.001 level.

studies and unpublished data across various aquatic ecosystems, including rivers (n = 628), estuaries (n = 530), and oceans (n = 1695) (see detailed data composition in Table S2).[41−50] All data with assigned formulas were combined and incorporated to establish the DOM molecular database. For the identification of MPs-DOM, the characteristic molecules of MPs-DOM with a significantly relative intensity-increased trend along with aging period were selected and then matched with our database based on their formula. This comprehensive data set provides a robust basis for identifying MPs-DOM molecules and probing the latent contribution (at the molecular level) of MPs-DOM to carbon cycling across the river-to-ocean continuum.

Statistical Analysis. R studio (v 4.3.3), IBM SPSS Statistics (v 25.0.0), and OriginPro 2023 (v 10.05) were used for data analysis and graphing. One-way analysis of variance (ANOVA) and Student's t-test were applied to test the significant difference of bulk parameters between different groups. Principal coordinates analysis (PCoA) and analysis of similarities (ANOSIM) were conducted to evaluate the similarity of MPs-DOM components between the treatments based on the Bray−Curtis distance. Linear regression analyses were used to evaluate relationships between molecular properties and aging times with a significance threshold of P < 0.05. A correlation between the relative intensities of MPs-DOM molecules and aging duration was considered statistically robust with Spearman's correlation coefficient (R) > 0.5 and P < 0.05.

RESULTS AND DISCUSSION

Physicochemical Properties of Virgin and Weathered MPs. The surface morphology of MPs before and after aging was examined by SEM. As shown in Figure 1a,b, virgin MPs displayed a relatively smooth surface, while an obvious rough structure with visible cracks appeared on 180 day weathered MPs. The distinct morphology of MPs depended on their types and sizes. Specifically, the surface of PE exhibited pores and protrusions (Figure 1a) but PP displayed significant pits (Figure 1b), which was in line with previous studies.[51,52] Notably, MPs with small sizes (i.e., PE-S and PP-S) exhibited coarser surfaces compared with that of large MPs (i.e., PE-L and PP-L) (Figure 1a,b), which was attributed to the enhanced mechanical abrasion between particles owing to their elevated specific surface area.[53] Furthermore, the variation of chemical functional groups obtained from the FTIR spectra provided direct evidence of aging and oxidation in the MPs. Virgin MPs displayed standard infrared peaks of PE and PP, whereas abundant oxygen-containing functional groups (e.g., carbonyl (∼1712 cm^{-1}) and hydroxyl group (∼3400 cm^{-1})) emerged on the MP surfaces following the 180 day weathering (Figure 1c,d). In addition, a new peak at 1104 cm^{-1} (stretching vibration of aliphatic C−O) appeared for PE after 180 day photoaging (Figure 1c), which was mainly attributed to the attack of alkoxy radical.[54] However, the diminishing peak at 1167 and 973 cm^{-1} (rocking vibration of CH_3) and emerging peak at 1103 cm^{-1} (stretching vibration of aliphatic C−O) were observed for PP following the 180 day weathering (Figure 1d), indicating the vital role of alkyl and hydroxyl radicals in polymer chain scission.[53] The oxidation degree of MPs under various weathering conditions was quantitatively evaluated using the carbonyl index (CI).[55] In this study, we observed a successional increase in CI values for PE-L, PE-S, PP-L, and PP-S after the 180 day aging, reaching 0.38 ± 0.07, 0.44 ± 0.05, 0.87 ± 0.17, and 1.14 ± 0.20, respectively (Figures 1e,f and S2). It is noteworthy that PP had significantly higher CI values than PE (Figure S2) (P < 0.05), with MP size further affecting their CI values. Specifically, weathered PE with large and small diameters displayed close CI values (Figure 1e),

https://doi.org/10.1021/acs.est.5c04083
Environ. Sci. Technol. 2025, 59, 18846−18856

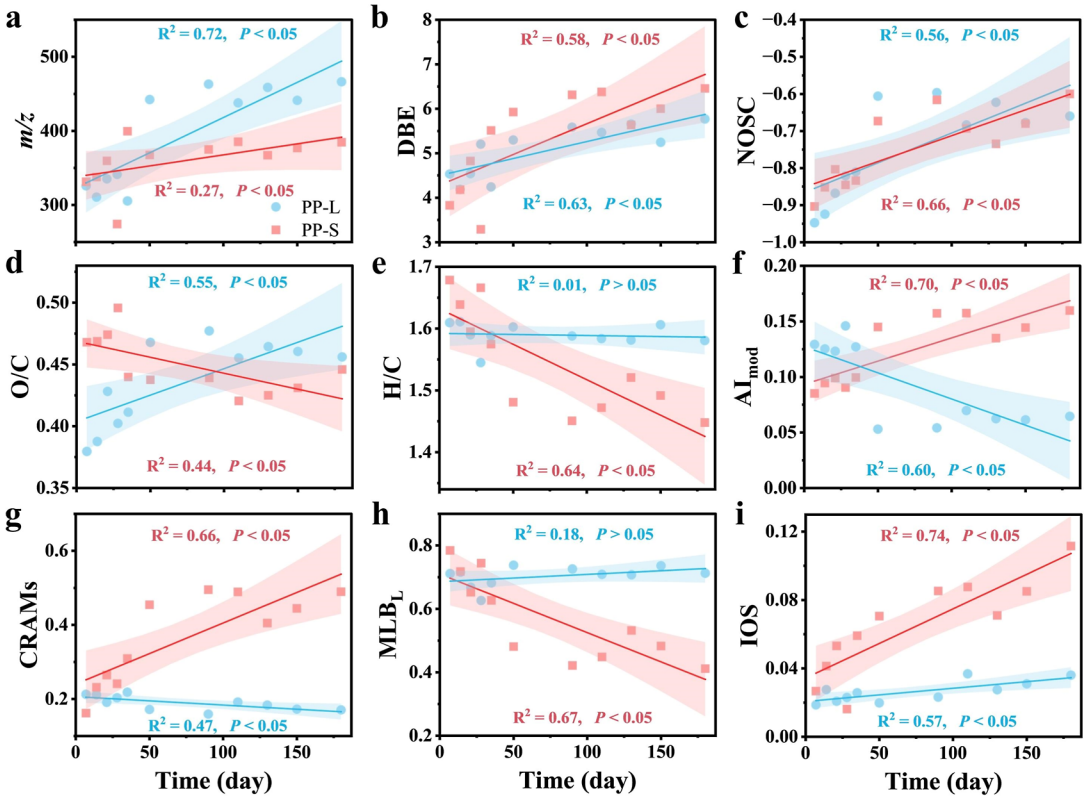

Figure 3. Bulk molecular indexes as a function of aging time. Comparison of (a) *m/z*, (b) DBE, (c) NOSC, (d) O/C, (e) H/C, (f) AI_{mod}, (g) CRAMs, (h) MLB_L, and (i) IOS between PP-L and PP-S MPs-DOM during 180 day artificial weathering periods. All FT-ICR MS molecular parameters are intensity-weighted values. All data were fitted using a linear regression model, with *R*-square (R^2) and *P* values obtained. The shaded region represents a 95% confidence interval.

while the CI value of PP-S was significantly higher than that of PP-L (Figure 1f) ($P < 0.05$). Such results indicated that the photoactivity of MPs followed the order of PP-S > PP-L > PE-S > PE-L, which could be attributed to differences in their chemical structures and sizes. Every other carbon atom in the PP backbone is a tertiary carbon, making it more prone to abiotic attack (e.g., UV irradiation and thermal oxidation) than the secondary carbons in PE.[17] In addition, the maximum sensitivity determined by the bond dissociation energies also follows the order of PE (96 kcal/mol at 300 nm) > PP (77 kcal/mol at 370 nm), indicating that less energy is required to dissociate chemical bonds (e.g., C−C and C−H) in PP than PE.[52] Furthermore, it has been reported that surface to volume ratio of the particle increases with the decrease in particle diameter.[16] The elevated specific surface area further increased the contact interface between PP and light, which might result in more production of free radicals (Figure S3) and consequently accelerate MP photodegradation.[53] However, PE has relatively lower photoreactivity, and even the elevated specific surface area failed to increase the production of more free radicals (Figure S3), resulting in similar chemical oxidation and FTIR profiles between PE-L and PE-S.

Changes of MPs-DOM Contents and Fluorescent Characteristics. Plastic type and size showed a pronounced influence on altering the MPs-DOM contents and compositions under long-term weathering periods. As shown in Figure 2a and b, weight-normalized DOC concentrations significantly increased with the extension of irradiation time for both PE and PP, while distinct trends were observed for various MPs and sizes. Specifically, PP can generally release more MPs-DOM than PE, and the leaching ratios of PE-S (0.015) and PP-S (0.081) were significantly higher than those of PE-L (0.007) and PP-L (0.016), respectively (Figure S4) ($P < 0.001$), which was comparable with previous studies.[19,51] At the end of aging (180 d), the final averaged DOC content of PP-S (14.38 ± 0.42 mg-C/g) was significantly higher than those of PP-L (2.53 ± 0.31 mg-C/g), PE-S (2.52 ± 0.19 mg-C/g), and PE-L (1.16 ± 0.16 mg-C/g) (Figure S5a) ($P < 0.05$). However, DOC concentrations of all MPs remained at very low levels under dark (<0.02 mg-C/g) (Figure S6a). Such results demonstrated that the increase of DOC originated from MP aging. A previous study reported that MPs floating at the surface of seawater contribute to about 260−23,600 t of DOC annually; the values were estimated based on the results of dark or 30 day light exposure.[16] The experimental conditions (e.g., MP types/concentrations, UV-exposure intensity, and artificial seawater) in our study and the above published literature were similar, and consequently, their results were comparable. However, our results showed that the DOC concentrations at 180 days were 10−150 times higher than that in dark or 30 day light conditions. By considering the difference of light exposure duration and intensity, scaling factors with values of 18.9−284.5 were applied in this study. Therefore, given the same weight of plastic waste in surface seawater, the estimated DOC contents released from buoyant MPs can reach 4,914−6,714,200 tons annually (details of DOC estimation are provided in Text S7). Such values were comparable with the DOM content in surface seawater (top 40 μm of the water column) and consequently increased marine organic carbon storage and diversity.[56]

https://doi.org/10.1021/acs.est.5c04083
Environ. Sci. Technol. 2025, 59, 18846−18856

The fluorescent characteristics of MPs-DOM were further investigated by using EEM- PARAFAC analysis. As shown in Figure S7, five fluorescent components were identified as protein-like substances (C1 and C2) and humic-like substances (C3, C4, and C5). The fluorescent intensity of C1−C5 basically increased with the extension of irradiation time for both PE and PP, which displayed similar trends for a_{254} (Figure S8). However, a_{254} and the fluorescent intensity of C1−C5 for all MPs remained at very low levels and showed insignificant changes before and after incubation under dark (Figure S6b−g). Such results indicated that photodegradation greatly contributed to the release of chromophoric DOM and fluorescent DOM from MPs to seawater. Notably, during the irradiation, the relative abundance of protein-like substances (C1−C2) increased from 29% to 50%, but the percentage of humic-like substances (C3−C5) decreased from 71% to 49% in PP-L (Figure 2c). Differently, in PP-S, the percentage of C1−C2 initially increased from 64% to 88% but gradually decreased to 34%, and the percentage of C3−C5 initially decreased from 36% to 12% but gradually increased to 66% (Figure 2d). Such temporal trend reversal was mainly attributed to the different release levels of each component at various aging periods (Figure S8a−d). However, the relative abundance of protein-like substances (C1−C2) increased from ∼30% to ∼70%, but the percentage of humic-like substances (C3−C5) decreased from 65% to 25% in PE-L and PE-S (Figure S9a,b). Furthermore, to better understand the variation of the DOM properties, three fluorescent indices were calculated. As shown in Figure 2e,f, HIX values in PE MPs-DOM slightly decreased with aging time extension, while the opposite trend was observed for PP MPs-DOM (especially for PP-S). At the end of irradiation (180 d), the final HIX values of PP-S (0.71 ± 0.08) were significantly higher than those of PP-L (0.64 ± 0.05), PE-L (0.39 ± 0.04), and PE-S (0.31 ± 0.03) (Figure S5d) ($P < 0.05$). However, FI and BIX decreased with extended aging time for PE and PP, and final values followed the order of PE-S > PE-L > PP-L > PP-S (Figures S5b,c and S9c−f) ($P < 0.05$). Notably, three fluorescent indices for all MPs basically remained unchanged before and after incubation in the dark (Figure S6h−j). Such results might be attributed to the difference of MPs' photochemical activity.[19,57] MPs-DOM derived from MPs with higher photochemical activity (i.e., PP-S) could be rapidly transformed from a protein-like component to humic/fulvic-like substances, while protein-like substances might be persistently produced for MPs with lower photochemical activity (i.e., PE-L, PE-S, and PP-L).

Temporally Dynamic Features of MPs-DOM Molecular Chemodiversity. The detailed MPs-DOM variations at the molecular level in different groups were further elucidated by FT-ICR MS. The molecular compositions of MPs-DOM basically remained unchanged at the initial and end of dark treatments (Figures S10−S13), while UV exposure significantly altered the dynamic features of MPs-DOM, as reflected by PCoA analysis (ANOSIM test, R = 0.582, $P = 0.001$) (Figures 3, S14 and S15). As the extension of aging duration, a significant increase of m/z, DBE, and NOSC values was observed for both PP-L and PP-S (Figure 3a−c) ($P < 0.05$). However, O/C and H/C values increased or slightly decreased for PP-L ($P > 0.05$) but significantly decreased for PP-S with the aging times, whereas AI_{mod} values remarkably decreased and increased for PP-L and PP-S, respectively (Figure 3d−f) ($P < 0.05$). CRAMs widely exist in the ocean and constitute the central part of the refractory dissolved organic matter (RDOM) pool.[37] The relative intensity of CRAMs significantly increased from ∼0.2 to ∼0.5 for PP-S with the aging time, which was greatly higher than that of PP-L, decreasing from ∼0.2 to ∼0.15 (Figure 3g) ($P < 0.05$). Furthermore, we employed MLB_L (higher values indicate greater biodegradability) and IOS (higher values indicate greater DOM stability) indexes to indicate the evolution of MPs-DOM stability. As shown in Figure 3h,i, significant increases and decreases were observed for MLB_L and IOS values ($P < 0.05$), respectively, as the PP-S weathering, whereas inapparent changes occurred in PP-L during this period ($P > 0.05$). Unlike PP, PE-L and PE-S exhibited the same variation tendency, as shown in Figure S14. The prolonged UV irradiation resulted in significant increases of O/C, m/z, NOSC, and MLB_L values ($P < 0.05$), while remarkably downward values of AI_{mod} and CRAMs were observed for PE ($P < 0.05$). These results showed that MPs-DOM was rapidly transformed from protein-like component to humic-like substances for PP-S,[18] which was significantly different from those for PP-L, PE-L, and PE-S ($P < 0.05$) (Figures S16 and S17).

To further reveal the temporally dynamic features of MPs-DOM, all samples were operationally divided into three stages according to exposure intervals, such as the early stage (7−35 days), middle stage (50−110 days), and late stage (130−180 days). Overall, most of the molecular indexes (except for H/C, MLB_L, and IOS) showed significant changes from early stage to middle or late stage but remained stable from middle stage to late stage both for PE (ANOSIM test, R = 0.359, $P = 0.002$) and PP (ANOSIM test, R = 0.21, $P = 0.024$), as proved by PCoA analysis (Figures S18−21). Specifically, O/C significantly increased from early stage to middle or late stage ($P < 0.01$), but H/C kept unchanged in these periods for PP-L, whereas both O/C and H/C distinctively descended from early stage to middle or late stage for PP-S (Figure S18a,b) ($P < 0.05$ or 0.01). AI_{mod} significantly decreased from early stage to middle or late stage for PP-L, but the value notably increased in these periods for PP-S (Figure S18c) ($P < 0.001$). In addition, m/z significantly increased from early stage to middle or late stage for PP-L ($P < 0.001$), but the index kept unchanged in these periods for PP-S (Figure S18d). However, DBE and NOSC indexes significantly increased from early stage to middle or late stage for both PP-L and PP-S (Figure S18e,f) ($P < 0.05$, 0.01, or 0.001). CRAMs significantly declined from early stage to middle or late stage for both PP-L ($P < 0.05$ or 0.01), but the obvious elevation was observed for PP-S ($P < 0.01$ or 0.001) (Figure S18g). Notably, the MLB_L and IOS values basically remained stable for PP-L during three stages, while these two indexes were subjected to prominent decline and increase from early stage to middle or late stage, respectively, for PP-S (Figure S18h,i) ($P < 0.05$, 0.01, or 0.001). Unlike PP, although the prolonged UV irradiation led to lower m/z, DBE, and NOSC ($P < 0.05$ or 0.01) for PE-S compared with PP-L, most molecular indexes (e.g., O/C, H/C, AI_{mod}, CRAMs, MLB_L, and IOS) for PE-L and PE-S at three stages exhibited the similar variation tendency as represented in Figures S19 and S21.

Molecular Fingerprints of Accumulated MPs-DOM Components. As the persistent DOM would play a vital role in regulating marine carbon cycle,[58] the relative intensity-increased MPs-DOM (RIIM) molecules generated during the aging period were emphatically investigated in the current study. As shown in Figures 4a, S23a and Table S3, the number

https://doi.org/10.1021/acs.est.5c04083
Environ. Sci. Technol. 2025, 59, 18846−18856

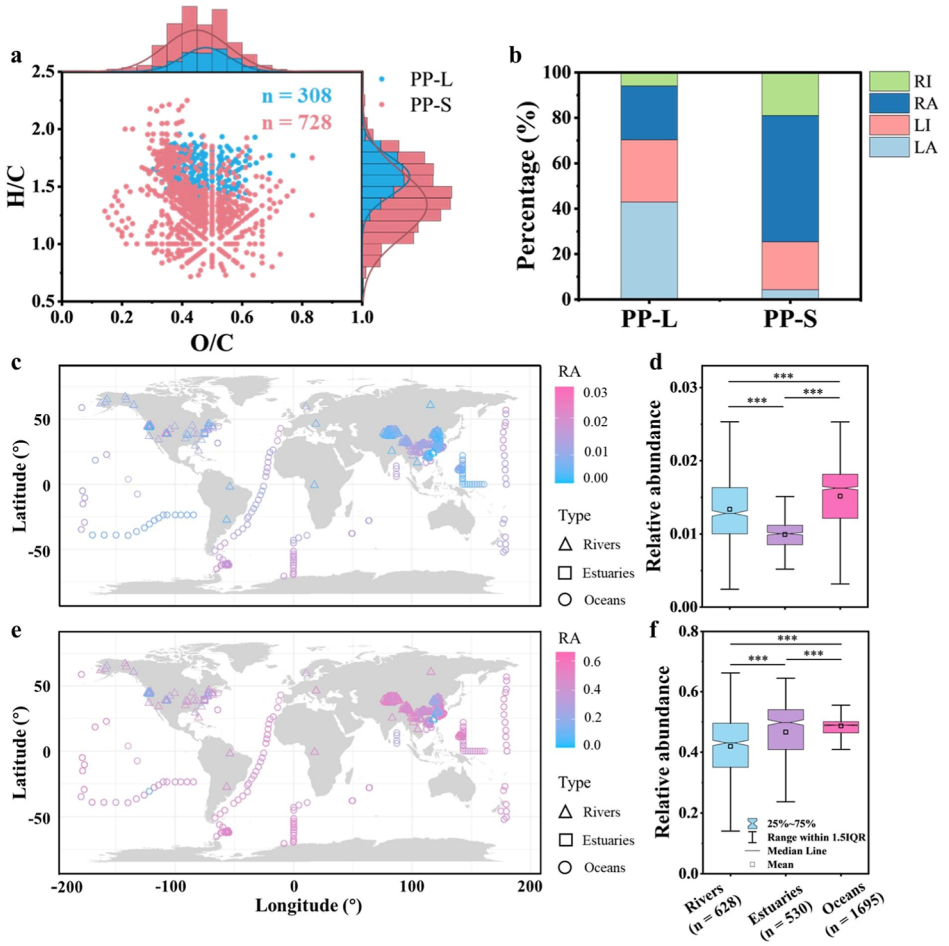

Figure 4. Characteristics and projection of relative intensity-increased MPs-DOM (RIIM) molecules across three aging periods. (a) Marginal van Krevelen diagrams showing the distribution of RIIM molecules derived from PP-L and PP-S during 180 day artificial weathering. (b) Relative abundance of four partitioned fractions (i.e., labile-active (LA), recalcitrant-active (RA), recalcitrant-inactive (RI), and labile-inactive (LI) molecules) for RIIM molecules derived from PP-L (n = 303) and PP-S (n = 728) based on the molecular reactivity and activity. Distribution of the sample sites and the matching ratio of RIIM molecules derived from (c) PP-L and (e) PP-S across three aging periods. Relative abundance of RIIM molecules derived from (d) PP-L and (f) PP-S matching in global rivers, estuaries, and oceans. Note that all match results are based on the molecular level. A significant difference is indicated at the *P < 0.05, **P < 0.01, or ***P < 0.001 level.

of MPs-DOM molecules with significantly upward trends (by relative intensity) for PP-S, PP-L, PE-S, and PE-L was 728, 308, 279, and 353, respectively. None of them were detected in blank (artificial seawater) and dark control samples, further confirming their molecular specificity. In addition, the bulk indexes of these fingerprint molecules were compared, and the results showed that the increasing MPs-DOM of PP-S possessed lower O/C, H/C, and m/z but higher NOSC, AI_{mod}, and DBE values than those of PP-L based on statistical analysis (Figure S22a–f and Table S3) (P < 0.001). The potential biochemical transformation analysis was conducted to further deepen the understanding of MPs-DOM turnover. According to their reactivity and activity, all RIIM molecules were parsed into four fractions: labile-active (LA), labile-inactive (LI), recalcitrant-active (RA), and recalcitrant-inactive (RI).[40] For PP-L, LA molecules had the highest relative abundance (by total molecule number) with the value of 42.9%, followed by LI (27.4%), RA (23.8%), and RI molecules (5.9%). However, the relative abundance of different groups for PP-S followed the order of RA (55.5%) > LI (21.2%) > RI (19.1%) > LA (4.3%) (Figure 4b). The same analysis was conducted for PE and the results are presented in Figure S23. Notably, the RIIM molecules of PE-L had higher O/C and NOSC values than those of PE-S (Figures S23b,g and Table S3) (P < 0.001), whereas no significant difference for H/C, m/z, DBE, and AI_{mod} was observed between PE-L and PE-S (Figure S23c–f). Potential biochemical transformation analysis of RIIM molecules of PE-L and PE-S exhibited similar results compared with those of PP-L. LA molecules had the highest relative abundance, ranging from 46.4% to 77.2%, followed by LI (17.7%–33.1%), RA (3.9%–11%), and RI molecules (1.2%–9.5%) (Figure S23h). Such results indicated that MPs-DOM derived from MPs with higher photochemical activity (i.e., PP-S) was rapidly transformed from a bioavailable component to bioinert substances, while MPs-DOM derived from weakly photochemical MPs (i.e., PE-L, PE-S, and PP-L) have relatively higher bioavailability.

Molecular Projection of Accumulated MPs-DOM Molecules onto Global Aquatic DOM Molecular Fingerprint Database. The persistent RIIM molecules were further matched and projected onto an established aquatic DOM molecular fingerprint database to probe the latent contribution of MPs-DOM to carbon cycling across the river-to-ocean continuum (Figures 4c–f and S24). After matching with the

https://doi.org/10.1021/acs.est.5c04083
Environ. Sci. Technol. 2025, 59, 18846–18856

database, relative abundance (RA), representing the percentage of RIIM molecules in the natural water samples was obtained. As shown in Figure 4c, only a small part of RIIM molecules derived from PP-L were matched in the DOM database, with the RA values ranging from 0.002 to 0.028. Results obtained from statistical analysis showed that the RA values of RIIM molecules derived from PP-L were significantly higher in open oceans than those in rivers and estuaries (Figure 4d) ($P < 0.001$). However, the remarkably higher matching ratios (RA values ranging from 0.04 to 0.66) were observed for RIIM molecules derived from PP-S, and the RA values across different ecosystems followed the order of oceans > estuaries > rivers (Figure 4e,f) ($P < 0.001$). Unlike PP, the RIIM molecules derived from PE-L and PE-S exhibited similar matching ratios with RA ranges of 0.004−0.19 and 0.01−0.28, respectively (Figure S24a,c). In addition, the RA values of RIIM molecules derived from PE-L were significantly higher in open oceans and estuaries than in rivers (Figure S24b) ($P < 0.001$). In contrast, the values for PE-S followed the order of estuaries > oceans > rivers (Figure S24d) ($P < 0.01$ or 0.001). Although MPs-DOM molecules were matched with natural aquatic DOM, identical formulas do not represent the same chemical structure. However, such significant overlap still highlights that plastic pollution might contribute to the marine carbon pool, which potentially affects organic carbon turnover and CO_2 release, etc.[16] In addition, to better understand the unique role of MPs-DOM in marine environments, more advanced technologies (e.g., LC-FT-ICR MS and FT-ICR MS/MS) will be employed to identify their structural information (e.g., the isomer cluster and functional group) in future studies.

Environmental Implications. Oceans serve as the final and largest sinks for global MPs, and the UV-induced photodissolution of MPs is prevalent in marine environments. Insight into the effects of MP inherent properties on the release and transformation of MPs-DOM under long-term sunlit seawater is important for understanding the marine carbon-neutrality strategy involving plastics. This study used ESI-FT-ICR MS to address the dynamic evolution of MPs-DOM derived from MPs with different chemical structures and sizes during persistent weathering periods and their potential influence on marine carbon cycles. Results demonstrated that MPs-DOM derived from MPs with higher photochemical activity (i.e., PP-S) might significantly contribute to the RDOM pool, whereas the accumulated MPs-DOM derived from weakly photochemical MPs (i.e., PE-L, PE-S, and PP-L) possesses higher bioavailability. Such labile MPs-DOM may finally be transformed into refractory components (e.g., CRAMs) due to the role of microbial carbon pump.[59] Based on our normalized DOC leaching ratio, the estimated amount of DOC contents released from buoyant MPs can reach 4,914−6,714,200 tons annually, which was comparable with the DOM content in surface seawater (top 40 μm of the water column). Such considerable and distinctive MPs-DOM can significantly affect marine carbon cycling, e.g., microbial activity, organic carbon storage, and CO_2 emission. In addition, small MPs exhibited higher levels of DOC release and RDOM accumulation in comparison to large particles. Notably, plastic debris in marine environments undergoes various natural processes and is gradually broken down into MPs and even NPs. Once degraded into NPs, the surface properties (e.g., surface energy, chemical activity, and heterogeneity) of plastics would greatly change, which might significantly accelerate the leaching of DOC. Therefore, we hypothesized that NPs might be a critical point from MPs transforming to MPs-DOM, which should be considered in future studies to comprehensively evaluate the effects of MP pollution on marine organic carbon storage. While photodegradation dominates MPs-DOM release in surface seawaters, the potential synergy with biodegradation under long-term aging across different plastic size classes should also be considered, given the vital role of microbes in marine carbon cycling. Although pure polymers were used in this study, various additives (e.g., antioxidants, plasticizers, and flame retardants) can be added to plastic products in real manufacture to improve their performance. Such a difference might potentially affect MP degradation pathways and MPs-DOM release kinetics, which merits more attention in future studies. Furthermore, as MPs photodegrade, various additives can also be released into water bodies. These chemicals are reported to have ecotoxicity on marine microorganisms serving as crucial primary producers (e.g., bacteria, algae, and zooplankton), finally, in turn, imposing profound effects on marine carbon cycling, which should be more attended in future studies.

■ ASSOCIATED CONTENT

Supporting Information

The Supporting Information is available free of charge at https://pubs.acs.org/doi/10.1021/acs.est.5c04083.

Details of aging experiments and MP Characterization; calculation of three fluorescent indices; sample preparation and calculation of key parameters of FT-ICR MS; details of biochemical transformation analysis and estimation of DOC content released from MPs; comparison of carbonyl index and •OH; comparison of DOC, FI, BIX, and HIX; variation of fluorescent components and a_{254}; additional FT-ICR MS results of MPs-DOM; principal coordinate analysis of MPs-DOM profiles; variation and significance analysis of bulk molecular indexes at three different aging periods; number and bulk indexes of RIIM molecules; molecular projection of RIIM molecules derived from PE onto global rivers, estuaries, and oceans; and data source of molecular fingerprint database (PDF)

Formula table of the RIIM molecules (XLSX)

■ AUTHOR INFORMATION

Corresponding Authors

Zhao Liang Chen − *Department of Ocean Science and Center for Ocean Research in Hong Kong and Macau, The Hong Kong University of Science and Technology, Hong Kong 999077, China;* orcid.org/0000-0002-5755-574X; Email: chenzl@ust.hk

Ding He − *Department of Ocean Science and Center for Ocean Research in Hong Kong and Macau, The Hong Kong University of Science and Technology, Hong Kong 999077, China; State Key Laboratory of Marine Pollution and Department of Chemistry, City University of Hong Kong, Kowloon 999077, China;* orcid.org/0000-0001-9620-6115; Email: dinghe@ust.hk

Authors

Yan-Jun Liu − *Department of Ocean Science and Center for Ocean Research in Hong Kong and Macau, The Hong Kong*

https://doi.org/10.1021/acs.est.5c04083
Environ. Sci. Technol. 2025, 59, 18846−18856

University of Science and Technology, Hong Kong 999077, China

Zekun Zhang − *Department of Ocean Science and Center for Ocean Research in Hong Kong and Macau, The Hong Kong University of Science and Technology, Hong Kong 999077, China*

Yuanbi Yi − *Department of Ocean Science and Center for Ocean Research in Hong Kong and Macau, The Hong Kong University of Science and Technology, Hong Kong 999077, China;* orcid.org/0000-0001-8420-8025

Ruanhong Cai − *Department of Ocean Science and Center for Ocean Research in Hong Kong and Macau, The Hong Kong University of Science and Technology, Hong Kong 999077, China*

Ming Ye − *Department of Ocean Science and Center for Ocean Research in Hong Kong and Macau, The Hong Kong University of Science and Technology, Hong Kong 999077, China*

Mengyang Liu − *State Key Laboratory of Marine Pollution and Department of Chemistry, City University of Hong Kong, Kowloon 999077, China;* orcid.org/0000-0001-9116-0453

Meng Yan − *State Key Laboratory of Marine Pollution and Department of Chemistry, City University of Hong Kong, Kowloon 999077, China;* orcid.org/0000-0002-5992-3171

Kenneth Mei Yee Leung − *State Key Laboratory of Marine Pollution and Department of Chemistry, City University of Hong Kong, Kowloon 999077, China;* orcid.org/0000-0002-2164-4281

Tanveer M. Adyel − *Centre for Nature Positive Solutions, School of Science, RMIT University, Melbourne, VIC 3000, Australia*

Complete contact information is available at: https://pubs.acs.org/10.1021/acs.est.5c04083

Notes

The authors declare no competing financial interest.

■ ACKNOWLEDGMENTS

We sincerely thank Prof. JIAO Nianzhi, Prof. ZHANG Chuanlun, Prof. FENG Xiaojuan, Prof. SHI Quan, Prof. SONG Kaishan, Prof. WANG Junjian, Prof. QI Yulin and Prof. ZHOU Yongqiang for sharing the valuable molecular fingerprint data. This work was supported by the National Key Research and Development Program of China (2023YFC3210200), the National Science Foundation of China (42222061), grants from the Research Grants Council of the Hong Kong Special Administrative Region, China (AoE/P-601/23 N and 16306623), the State Key Laboratory of Marine Pollution (SKLMP) Seed Collaborative Research Fund (SKLMP/SCRF/0044), the Marine Ecology Enhancement Fund of Hong Kong (MEEF2024011), and the Center for Ocean Research in Hong Kong and Macau (CORE). CORE is a joint research center for ocean research between Laoshan Laboratory and HKUST. TMA was supported by an Australian Research Council Discovery Early Career Researcher Award (DECRA, DE240100633) grant and the 2024 Thomas Davies Research Grant for Marine, Soil and Plant Biology from the Australian Academy of Science.

■ REFERENCES

(1) Bank, M. S.; Hansson, S. V. The Plastic Cycle: A novel and holistic paradigm for the anthropocene. *Environ. Sci. Technol.* **2019**, *53* (13), 7177−7179.

(2) PlasticsEurope. Plastics − the fast Facts 2024. Plastics Europe, 2024, https://plasticseurope.org/knowledge-hub/plastics-the-fast-facts-2024/.

(3) Kaandorp, M. L. A.; Lobelle, D.; Kehl, C.; Dijkstra, H. A.; van Sebille, E. Global mass of buoyant marine plastics dominated by large long-lived debris. *Nat. Geosci.* **2023**, *16* (8), 689−694.

(4) MacLeod, M.; Arp, H. P. H.; Tekman, M. B.; Jahnke, A. The global threat from plastic pollution. *Science* **2021**, *373* (6550), 61−65.

(5) Strokal, M.; Vriend, P.; Bak, M. P. P.; Kroeze, C.; van Wijnen, J.; van Emmerik, T. River export of macro- and microplastics to seas by sources worldwide. *Nat. Commun.* **2023**, *14* (1), 4842.

(6) Ter Halle, A.; Ladirat, L.; Gendre, X.; Goudouneche, D.; Pusineri, C.; Routaboul, C.; Tenailleau, C.; Duployer, B.; Perez, E. Understanding the fragmentation pattern of marine plastic debris. *Environ. Sci. Technol.* **2016**, *50* (11), 5668−5675.

(7) Marcharla, E.; Vinayagam, S.; Gnanasekaran, L.; Soto-Moscoso, M.; Chen, W. H.; Thanigaivel, S.; Ganesan, S. Microplastics in marine ecosystems: A comprehensive review of biological and ecological implications and its mitigation approach using nanotechnology for the sustainable environment. *Environ. Res.* **2024**, *256*, 119181.

(8) Cole, M.; Lindeque, P.; Fileman, E.; Halsband, C.; Goodhead, R.; Moger, J.; Galloway, T. S. Microplastic ingestion by zooplankton. *Environ. Sci. Technol.* **2013**, *47* (12), 6646−6655.

(9) Wardrop, P.; Shimeta, J.; Nugegoda, D.; Morrison, P. D.; Miranda, A.; Tang, M.; Clarke, B. O. Chemical pollutants sorbed to ingested microbeads from personal care products accumulate in fish. *Environ. Sci. Technol.* **2016**, *50* (7), 4037−4044.

(10) Watts, A. J. R.; Urbina, M. A.; Corr, S.; Lewis, C.; Galloway, T. S. Ingestion of plastic microfibers by the crab Carcinus maenas and its effect on food consumption and energy balance. *Environ. Sci. Technol.* **2015**, *49* (24), 14597−14604.

(11) Peng, R.; Xu, Y.; Li, R.; Wang, W.; Wang, H.; Zhang, X.; Yuan, Q. Marine microplastics enrich antibiotic resistance genes (ARGs), especially extracellular ARGs: An investigation in the East China Sea. *Mar. Pollut. Bull.* **2024**, *209* (Part B), 117260.

(12) Liu, G.; Zhu, Z.; Yang, Y.; Sun, Y.; Yu, F.; Ma, J. Sorption behavior and mechanism of hydrophilic organic chemicals to virgin and aged microplastics in freshwater and seawater. *Environ. Pollut.* **2019**, *246*, 26−33.

(13) Gao, F.; Li, J.; Sun, C.; Zhang, L.; Jiang, F.; Cao, W.; Zheng, L. Study on the capability and characteristics of heavy metals enriched on microplastics in marine environment. *Mar. Pollut. Bull.* **2019**, *144*, 61−67.

(14) Hansell, D. A.; Carlson, C. A.; Repeta, D. J.; Schlitzer, R. Dissolved organic matter in the ocean a controversy stimulates new insights. *Oceanography* **2009**, *22* (4), 202−211.

(15) Moran, M. A.; Kujawinski, E. B.; Stubbins, A.; Fatland, R.; Aluwihare, L. I.; Buchan, A.; Crump, B. C.; Dorrestein, P. C.; Dyhrman, S. T.; Hess, N. J.; Howe, B.; Longnecker, K.; Medeiros, P. M.; Niggemann, J.; Obernosterer, I.; Repeta, D. J.; Waldbauer, J. R. Deciphering ocean carbon in a changing world. *Proc. Natl. Acad. Sci. U.S.A.* **2016**, *113* (12), 3143−3151.

(16) Romera-Castillo, C.; Pinto, M.; Langer, T. M.; Alvarez-Salgado, X. A.; Herndl, G. J. Dissolved organic carbon leaching from plastics stimulates microbial activity in the ocean. *Nat. Commun.* **2018**, *9*, 1430.

(17) Gewert, B.; Plassmann, M. M.; MacLeod, M. Pathways for degradation of plastic polymers floating in the marine environment. *Environ. Sci.: Processes Impacts* **2015**, *17* (9), 1513−1521.

(18) Stubbins, A.; Zhu, L.; Zhao, S.; Spencer, R. G. M.; Podgorski, D. C. Molecular signatures of dissolved organic matter generated from the photodissolution of microplastics in sunlit seawater. *Environ. Sci. Technol.* **2023**, *57* (48), 20097−20106.

(19) Zhu, L.; Zhao, S.; Bittar, T. B.; Stubbins, M.; Li, D. Photochemical dissolution of buoyant microplastics to dissolved

organic carbon: Rates and microbial impacts. *J. Hazard. Mater.* **2020**, *383*, 121065.
(20) Liu, Y.; Hu, Y.; Yang, C.; Chen, C.; Huang, W.; Dang, Z. Aggregation kinetics of UV irradiated nanoplastics in aquatic environments. *Water Res.* **2019**, *163*, 114870.
(21) Song, F.; Li, T.; Hur, J.; Shi, Q.; Wu, F.; He, W.; Shi, D.; He, C.; Zhou, L.; Ruan, M.; Cao, Y. Molecular-level insights into the heterogeneous variations and dynamic formation mechanism of leached dissolved organic matter during the photoaging of polystyrene microplastics. *Water Res.* **2023**, *242*, 120114.
(22) Law, K. L.; Annual, R. Plastics in the Marine Environment. *Annu. Rev. Mar. Sci.* **2017**, *9*, 205−229.
(23) van Sebille, E.; Wilcox, C.; Lebreton, L.; Maximenko, N.; Hardesty, B. D.; van Franeker, J. A.; Eriksen, M.; Siegel, D.; Galgani, F.; Law, K. L. A global inventory of small floating plastic debris. *Environ. Res. Lett.* **2015**, *10* (12), 124006.
(24) Chen, Z. L.; Yi, Y.; Cai, R.; Zhang, Z.-X.; Liang, W.; Fu, W.; Li, P.; Wang, K.; Zhang, L.; Dong, K.; Li, S.-L.; Xu, S.; He, D. Revealing the mobilization and age of estuarine dissolved organic matter during floods using radiocarbon and molecular fingerprints. *Water Res.* **2025**, *271*, 122898.
(25) Liu, M.; Liu, H. M.; Yang, K.; Li, J.; Huang, C.; Yang, J.; Chen, W.; Ying, K.; Leung, K. M. Y.; Zhang, K.; Xu, X.; Liao, R.; Yan, M. Advancing the understanding of microplastic weathering: insights from a novel polarized light scattering approach. *Environ. Sci. Technol.* **2024**, *58* (42), 19004−19015.
(26) Hansen, A. M.; Kraus, T. E. C.; Pellerin, B. A.; Fleck, J. A.; Downing, B. D.; Bergamaschi, B. A. Optical properties of dissolved organic matter (DOM): effects of biological and photolytic degradation. *Limnol. Oceanogr.* **2016**, *61* (3), 1015−1032.
(27) Gao, J.; Liang, C.; Shen, G.; Lv, J.; Wu, H. Spectral characteristics of dissolved organic matter in various agricultural soils throughout China. *Chemosphere* **2017**, *176*, 108−116.
(28) Pucher, M.; Wunsch, U.; Weigelhofer, G.; Murphy, K.; Hein, T.; Graeber, D. staRdom Versatile software for analyzing spectroscopic data of dissolved organic matter in R. *Water* **2019**, *11* (11), 2366.
(29) Liu, Y.-J.; Yang, H.-Y.; Gao, S.-X.; Li, Z.-H.; Hu, Y.-Y.; Zheng, X.; Sheng, G.-P. Molecular fractionation mediates genotoxicity evolution of hydrochar-derived dissolved organic matter at the iron oxyhydroxides-water interface. *Water Res.* **2025**, *268*, 122584.
(30) Yi, Y.; He, C.; Klaproth, K.; Merder, J.; Li, P.; Qi, Y.; Fu, P.; Li, S.; Dittmar, T.; Shi, Q.; He, D. Will various interpretation strategies of the same ultrahigh-resolution mass spectrometry data tell different biogeochemical stories? A first assessment based on natural aquatic dissolved organic matter. *Limnol. Oceanogr-Meth.* **2023**, *21* (6), 320−333.
(31) Koch, B. P.; Ludwichowski, K.-U.; Kattner, G.; Dittmar, T.; Witt, M. Advanced characterization of marine dissolved organic matter by combining reversed-phase liquid chromatography and FT-ICR-MS. *Mar. Chem.* **2008**, *111* (3−4), 233−241.
(32) Stenson, A. C.; Marshall, A. G.; Cooper, W. T. Exact masses and chemical formulas of individual Suwannee River fulvic acids from ultrahigh resolution electrospray ionization Fourier transform ion cyclotron resonance mass spectra. *Anal. Chem.* **2003**, *75* (6), 1275−1284.
(33) Kim, S.; Kramer, R. W.; Hatcher, P. G. Graphical method for analysis of ultrahigh-resolution broadband mass spectra of natural organic matter, the van Krevelen diagram. *Anal. Chem.* **2003**, *75* (20), 5336−5344.
(34) Fu, Q.-L.; Fujii, M.; Ma, R. Development of a Gaussian-based alignment algorithm for the ultrahigh-resolution mass spectra of dissolved organic matter. *Anal. Chem.* **2023**, *95*, 2796−2803.
(35) Kellerman, A. M.; Dittmar, T.; Kothawala, D. N.; Tranvik, L. J. Chemodiversity of dissolved organic matter in lakes driven by climate and hydrology. *Nat. Commun.* **2014**, *5*, 3804.
(36) D'Andrilli, J.; Cooper, W. T.; Foreman, C. M.; Marshall, A. G. An ultrahigh-resolution mass spectrometry index to estimate natural organic matter lability. *Rapid Commun. Mass Spectrom.* **2015**, *29* (24), 2385−2401.
(37) Lechtenfeld, O. J.; Kattner, G.; Flerus, R.; McCallister, S. L.; Schmitt-Kopplin, P.; Koch, B. P. Molecular transformation and degradation of refractory dissolved organic matter in the Atlantic and Southern Ocean. *Geochim. Cosm. Acta* **2014**, *126*, 321−337.
(38) Breitling, R.; Ritchie, S.; Goodenowe, D.; Stewart, M. L.; Barrett, M. P. Ab initio prediction of metabolic networks using Fourier transform mass spectrometry data. *Metabolomics* **2006**, *2* (3), 155−164.
(39) Danczak, R. E.; Chu, R. K.; Fansler, S. J.; Goldman, A. E.; Graham, E. B.; Tfaily, M. M.; Toyoda, J.; Stegen, J. C. Using metacommunity ecology to understand environmental metabolomes. *Nat. Commun.* **2020**, *11* (1), 6369.
(40) Hu, A.; Jang, K.-S.; Meng, F.; Stegen, J.; Tanentzap, A. J.; Choi, M.; Lennon, J. T.; Soininen, J.; Wang, J. Microbial and environmental processes shape the link between organic matter functional traits and composition. *Environ. Sci. Technol.* **2022**, *56* (14), 10504−10516.
(41) He, D.; Li, P.; He, C.; Wang, Y.; Shi, Q. Eutrophication and watershed characteristics shape changes in dissolved organic matter chemistry along two river-estuarine transects. *Water Res.* **2022**, *214*, 118196.
(42) Zhou, Y.; Yao, X.; Zhou, L.; Zhao, Z.; Wang, X.; Jang, K. S.; Tian, W.; Zhang, Y.; Podgorski, D. C.; Spencer, R. G. M.; Kothawala, D. N.; Jeppesen, E.; Wu, F. How hydrology and anthropogenic activity influence the molecular composition and export of dissolved organic matter: Observations along a large river continuum. *Limnol. Oceanogr.* **2021**, *66* (5), 1730−1742.
(43) Liu, T.; Wang, X.; Zhu, E.; Liu, Z.; Zhang, X.; Guo, J.; Liu, X.; He, C.; Hou, S.; Fu, P.; Shi, Q.; Feng, X. Evolution of the dissolved organic matter composition along the upper Mekong (Lancang) river. *ACS Earth Space Chem.* **2021**, *5* (2), 319−330.
(44) Kellerman, A. M.; Guillemette, F.; Podgorski, D. C.; Aiken, G. R.; Butler, K. D.; Spencer, R. G. M. Unifying concepts linking dissolved organic matter composition to persistence in aquatic ecosystems. *Environ. Sci. Technol.* **2018**, *52* (5), 2538−2548.
(45) Yi, Y.; Liu, T.; Merder, J.; He, C.; Bao, H.; Li, P.; Li, S.; Shi, Q.; He, D. Unraveling the linkages between molecular abundance and stable carbon isotope ratio in dissolved organic matter using machine learning. *Environ. Sci. Technol.* **2023**, *57* (46), 17900−17909.
(46) Riedel, T.; Zark, M.; Vahatalo, A. V.; Niggemann, J.; Spencer, R. G. M.; Hernes, P. J.; Dittmar, T. Molecular signatures of biogeochemical transformations in dissolved organic matter from ten world rivers. *Front. Earth Sci.* **2016**, *4*, 85.
(47) Ryan, K. A.; Garayburu-Caruso, V. A.; Crump, B. C.; Bambakidis, T.; Raymond, P. A.; Liu, S.; Stegen, J. C. Riverine dissolved organic matter transformations increase with watershed area, water residence time, and Damkohler numbers in nested watersheds. *Biogeochemistry* **2024**, *167* (10), 1203−1224.
(48) Osterholz, H.; Kirchman, D. L.; Niggemann, J.; Dittmar, T. Environmental drivers of dissolved organic matter molecular composition in the Delaware estuary. *Front. Earth Sci.* **2016**, *4*, 95.
(49) Zheng, X.; Cai, R.; Yao, H.; Zhuo, X.; He, C.; Zheng, Q.; Shi, Q.; Jiao, N. Experimental insight into the enigmatic persistence of marine refractory dissolved organic matter. *Environ. Sci. Technol.* **2022**, *56* (23), 17420−17429.
(50) Bercovici, S. K.; Wiemers, M.; Dittmar, T.; Niggemann, J. Disentangling biological transformations and photodegradation processes from marine dissolved organic matter composition in the global ocean. *Environ. Sci. Technol.* **2023**, *57* (50), 21145−21155.
(51) Tuttle, E.; Wiman, C.; Muñoz, S.; Law, K. L.; Stubbins, A. Sunlight-driven photochemical removal of polypropylene microplastics from surface waters follows linear kinetics and does not result in fragmentation. *Environ. Sci. Technol.* **2024**, *58* (12), 5461−5471.
(52) Song, Y. K.; Hong, S. H.; Jang, M.; Han, G. M.; Jung, S. W.; Shim, W. J. Combined effects of UV exposure duration and mechanical abrasion on microplastic fragmentation by polymer type. *Environ. Sci. Technol.* **2017**, *51* (8), 4368−4376.

https://doi.org/10.1021/acs.est.5c04083
Environ. Sci. Technol. 2025, 59, 18846−18856

(53) Wu, X.; Zhao, X.; Chen, R.; Liu, P.; Liang, W.; Wang, J.; Shi, D.; Teng, M.; Wang, X.; Gao, S. Size-dependent long-term weathering converting floating polypropylene macro- and microplastics into nanoplastics in coastal seawater environments. *Water Res.* **2023**, *242*, 120165.
(54) Liu, S.; Huang, W.; Yang, J.; Xiong, Y.; Huang, Z.; Wang, J.; Cai, T.; Dang, Z.; Yang, C. Formation of environmentally persistent free radicals on microplastics under UV irradiations. *J. Hazard. Mater.* **2023**, *453*, 131277.
(55) Veerasingam, S.; Ranjani, M.; Venkatachalapathy, R.; Bagaev, A.; Mukhanov, V.; Litvinyuk, D.; Mugilarasan, M.; Gurumoorthi, K.; Guganathan, L.; Aboobacker, V. M.; Vethamony, P. Contributions of Fourier transform infrared spectroscopy in microplastic pollution research: A review. *Crit. Rev. Environ. Sci. Technol.* **2021**, *51* (22), 2681−2743.
(56) Liu, X.; Fang, L.; Gardea-Torresdey, J. L.; Zhou, X.; Yan, B. Microplastic-derived dissolved organic matter: Generation, characterization, and environmental behaviors. *Sci. Total Environ.* **2024**, *948*, 174811.
(57) Zhang, J.; Hou, X.; Zhang, K.; Xiao, Q.; Gardea-Torresdey, J. L.; Zhou, X.; Yan, B. Photochemistry of microplastics-derived dissolved organic matter: Reactive species generation and organic pollutant degradation. *Water Res.* **2025**, *269*, 122802.
(58) Cai, R.; Jiao, N. Recalcitrant dissolved organic matter and its major production and removal processes in the ocean. *Deep Sea Res., Part I* **2023**, *191*, 103922.
(59) Jiao, N.; Herndl, G. J.; Hansell, D. A.; Benner, R.; Kattner, G.; Wilhelm, S. W.; Kirchman, D. L.; Weinbauer, M. G.; Luo, T.; Chen, F.; Azam, F. Microbial production of recalcitrant dissolved organic matter: long-term carbon storage in the global ocean. *Nat. Rev. Microbiol.* **2010**, *8* (8), 593−599.

https://doi.org/10.1021/acs.est.5c04083
Environ. Sci. Technol. 2025, 59, 18846−18856